J Nanopart Res (2020) 22: 169
https://doi.org/10.1007/s11051-020-04908-5

RESEARCH PAPER

$Li_2CoTi_3O_8$ and its composite nanofibers as high performance and long cycle lithium ion electrode materials

Yuzhou Liu · Shuiping Huang · Chao Wang · Nan Gao · Xiaoyang Qiu · Xing Li

Received: 17 January 2020 / Accepted: 5 June 2020 / Published online: 16 June 2020

Abstract In this work, $Li_2CoTi_3O_8$ nanofibers and $Li_2CoTi_3O_8$·$CoTiO_3$·TiO_2 (LCT) composite nanofibers as anode materials in lithium-ion batteries (LIBs) were successfully prepared by a traditional electrospinning technology, and characterized by X-ray diffraction (XRD), scanning electron microscopy (SEM), high-resolution transmission electron microscopy (HRTEM), energy-dispersive spectrometer (EDS), X-ray photoelectron spectroscopy (XPS), thermogravimetric analysis (TGA), and mappings. XRD confirms that the composite materials lattice planes well correspond to the patterns of $Li_2CoTi_3O_8$, $CoTiO_3$, and TiO_2, respectively. SEM and TEM exhibits the fabricated composites are one-dimensional nanofibers with the diameter of 250~300 nm and 150~200 nm after annealing, respectively. The electrochemical properties of the materials for LIBs are investigated to indicate that the (LCT) composite nanofibers hold high reversible capacity of 201.68 mAh g^{-1} after 120 cycles and high rate capability at different current densities.

Keywords Electrospinning · Composites · Anode materials · Lithium ion batteries · Nanomaterials · Energy storage

Electronic supplementary material The online version of this article (https://doi.org/10.1007/s11051-020-04908-5) contains supplementary material, which is available to authorized users.

Y. Liu · S. Huang (✉) · C. Wang · X. Li
School of Physical Science and Technology, Key Laboratory of Photoelectric Materials and Devices of Zhejiang Province, Ningbo University, Ningbo 315211, China
e-mail: huangshuiping@nbu.edu.cn

N. Gao · X. Qiu · X. Li (✉)
School of Materials Science and Chemical Engineering, State Key Laboratory Base of Novel Functional Materials and Preparation Science, Ningbo University, Ningbo 315211, China
e-mail: lixing@nbu.edu.cn

X. Qiu
State Key Laboratory of Structural Chemistry, Chinese Academy of Sciences, Fujian Institute of Research on the Structure of Matter, Fuzhou, Fujian 350002, People's Republic of China

Introduction

Nowadays, the global energy crisis and environmental concerns are becoming more serious due to the continuous economic development and population growth. To mitigate these troubles, development and utilization of renewable energies (e.g., solar, wind and tidal energy) have become the focus of researches in many countries. Lithium-ion batteries (LIBs) (Zeng et al. 2019; Han et al. 2019) account for the main part in energy storage devices owing to their high energy density, reliability, long service life, and low environmental pollution (Xu et al. 2007). LIBs have been widely used in portable devices, transport systems like electric car (EVs) (Huang et al. 2018) and hybrid electric vehicles (HEVs) (Cusenza et al. 2019) as the most advanced energy storage equipments. The anode materials of LIBs are usually used as the main body for storing Li^+, which directly determines the ability of lithium storage capability (Goriparti et al. 2014; Simon and Goswami 2011).

Graphites are the traditional anode materials because of its high theoretical capacity (372 mAh g^{-1}) (Zhang et al. 2019) and low cost. However, graphite's shortages have restricted its further application in LIBs such as the formation of solid electrolyte interface (SEI) film (Huff et al. 2016), which seriously hindered ion transportation. A low working voltage (0.1 V) of the graphite brings capacity fading and fearful safety problems during the rapidLi^+ lithiation/delithiation process. Therefore, it is very essential to develop new anode materials with higher stability and capacity in LIBs.

Except for traditional graphite anode materials, $Li_4Ti_5O_{12}$ (LTO) has been widely studied by scientists in the past three decades (Liu et al. 2019a, b; Tojo et al. 2019), which is regarded to be the most representative titanates. The spinel LTO has a high embedding potential of 1.55 V (vs. Li/Li^+) (Sandhya et al. 2014; Yi et al. 2014a, b) and can suppress the growth of lithium dendrites under high-rate charge/discharge. In addition, there is hardly volume change during the lithium insertion/extraction processes (Ahn and Xiao 2011). Consequently, LTO is a potential high-rate LIBs candidate. Nevertheless, the electronic conductivity of LTO is relatively low (Yuan et al. 2010) due to the 3D orbit of Ti element, which possibly leads to high polarization and capacities loss at higher cycle rates (Ouyang et al. 2007). In order to improve the electronic conductivity of LTO, three tactics are carried out as follows: (i) coating conductive materials on the surface of LTO (Xu et al. 2014; Wang et al. 2014); (ii) increasing the specific surface areas by changing the composites' morphology to be nanofibers (Serife et al. 2015; Jung et al. 2015) or nanoparticles (Kamali and Fray 2015; Railey et al. 2017); (iii) doping some metal elements (Na^+ (Yi et al. 2014a, b), Mg^{2+} (Lao et al. 2016), Co^{3+} (Wang et al. 2012), La^{3+} (Trong et al. 2015), Zr^{4+} (Hou et al. 2018), Ru^{4+} (Leng et al. 2019), Nb^{5+} (Tian et al. 2012), Sn^{2+} (He et al. 2017)) or non-metallic elements (F^- (Zhao et al. 2013), Br^- and W^- (Zhang et al. 2015)) to stabilize the framework structures. The disadvantages of nonuniform coating thickness would decrease the capacities of the battery. Note the electrospinning technology has currently attracted extensive attention for one-dimensional nanofibers (Bhardwaj and Kundu 2010). Much more researchers prefer this technique to enlarge specific surface area with the purpose of improving the utility of the active materials. According to the previous studies, $Li_2CoTi_3O_8$ nanofibers could be prepared by electrospinning technology to build the particular skeleton structures (Wang et al. 2012). In this paper, we adopt the means of electrospinning to fabricate a complex $Li_2CoTi_3O_8{\cdot}CoTiO_3{\cdot}TiO_2$ (LCT), which is used for the anode materials in LIBs. TiO_2 has played an important role in LIBs on account of its high structure stability, long cycle life, and prominent security (Cheng et al. 2020); the theoretical specific capacity of TiO_2 is 335 mAh g^{-1}. Meanwhile, $CoTiO_3$ has been reported as one of the anode materials, which performs a function of enhancing cycling life (Liu et al. 2019a, b). So, we intend to add Co elements into $Li_4Ti_5O_{12}$ to construct a novel kind of hierarchical nanohybrids LCT by electrospinning technology. According to last research studies, the theoretical specific capacity of $Li_2CoTi_3O_8$ is calculated as 233.5 mAh g^{-1} (Wang et al. 2013). In addition, compared with the $Li_2CoTi_3O_8$, the LCT as anode materials in LIBs display superior cycling stability and rate capability.

Experimental section

Preparation of materials

The LCT precursor composite nanofibers were fabricated through electrospinning, and then were treated by heating to get the final product. In a typical process, 0.4982 g cobalt tetrahydrate acetate (Macklin Chemical, 99.0%) was dissolved in 5 mL *N*,*N*-dimethylformamide (Macklin Chemical, 99.0%). In the meantime, 0.1320 g lithium acetate (Macklin Chemical, 99.9%) was added to the mixed solution of 5 mL absolute ethanol, 2 mL tetrabutyl titanate (Macklin Chemical, 99.0%), and 2 mL acetic acid (Macklin Chemical, 99.0%). The above solutions were mixed under vigorous magnetic stirring, and then 1.3802 g polyvinyl pyrrolidone (Aladdin Chemical, Mw = 1,300,000) was added into the hybrid solution with stirring constantly for 10 h to get the dark-red precursor solution for electrospinning.

The electrospinning experiments were carried out by loading the prepared mixture solution into a 10-mL plastic syringe with 17.0 kV and 15.0 cm of the vertical distance between the needle and the collector. The 0.6316 mL h^{-1} flow rate was employed at 35 °C. The nanofibers were collected into and dried at 80 °C for 4 h in a vacuum oven. The heated treatment included the preconditioning at 200 °C for 2 h with a heating rate of 2 °C min^{-1} and the calcining at 700 °C for 2 h with a heating rate of 3 °C min^{-1} under air atmosphere, which

aimed to remove the organic polymers and obtain LCT composite nanofibers. As a contrast, the $Li_2CoTi_3O_8$ nanofibers were prepared with the same stoichiometric ratio of cobalt tetrahydrate acetate, lithium acetate, and tetrabutyl titanate (Macklin Chemical, 99.0%) in the solvents. The schematic illustrations of the formation of LCT composite nanofibers and $Li_2CoTi_3O_8$ nanofibers are shown in Fig. 1. All the chemical regents are of analytical grade in the experiment and used without further purification.

Characterization

The structures of the samples were detected by X-ray diffraction (XRD, Bruker D8 Focus Advance) using Cu-Ka radiation with scan angles ranging from 10° to 70°. The morphologies were characterized by scanning electron microscopy (SEM, Hitachi, SU-70) and high-resolution transmission electron microscopy (HRTEM, JEOL, JEM-2010) at an accelerating voltage of 200 kV. Energy-dispersive spectrometer (EDS) testing was performed in TEM mode. The distributions of valence states were conducted by X-ray photoelectron spectroscopy (XPS, Al Kα radiation). Thermogravimetric analysis (TGA, SIITG/DTA 6300) was analyzed under air atmosphere from 25 to 720 °C (5 °C min^{-1}). The spinning process was accomplished by a FM1206 electrospinning machine (Beijing Fuyouma, China).

Electrochemical measurements

The CR2032-type coin cells were used to evaluate the electrochemical performances and the negative working electrodes consisted of active materials (LCT composite nanofibers or $Li_2CoTi_3O_8$ nanofibers), carbon black and polyvinylidene fluoride (PVDF) binder in a mass ratio of 8:1:1 (wt%). After fully grinded, the electrode slurry was eventually coated on a Cu metal foils and dried at 100 °C for 10 h in the vacuum oven with the average loading mass for each electrode being 1.5 ± 0.2 mg cm^{-2}. All the coin cells were assembled in an argon-filled glove box ($H_2O < 0.01$ ppm, $O_2 <$ 0.01 ppm). Celgard 2400 and pure Li metal foils were used as separator and the counter electrodes, respectively. The electrolyte was a pre-made solution of 1.0 M $LiPF_6$ solution in an ethylene carbonate (EC)/dimethyl carbonate (DMC) (1:1, v/v). Galvanostatic charge-discharge cycles were recorded on multichannel LAND-CT2001A battery test systems to measure coin cells at different current densities in the voltage range of 0.0~3.0 V. Electrochemical impedance spectroscopy (EIS, 0.01 ~ 100 kHz) and cyclic voltammetry (CV, 0.1 mV s^{-1}, 0.0 ~ 3.0 V) were operated on a CHI660D electrochemical working station. All the electrochemical analyses were carried out at a relatively constant temperature of 25 °C.

Results and discussion

The schematic illustration of the electrospinning and subsequent calcination process of one-dimensional nanofibers are described in Fig. 1, in which the diameter of the LCT composite nanofibers is 250~300 nm (Fig. S1) before sintered and that of the nanofibers is 150 to 200 nm after sintered at 700 °C in an air atmosphere, the $Li_2CoTi_3O_8$ nanofibers is 200~300 nm after sintered (Fig. S4). The high-resolution XPS spectra of the LCT composite nanofibers are exhibited in Fig. 2a–c to display the three different elements' binding energies of Co 2p, Ti 2p, and O 1s. It can be seen from the Co 2p spectrum (Fig. 2a), the Co 2p peak splits into Co $2p_{3/2}$ (780.5 eV), Co $2p_{3/2}$ (781.8 eV), and Co $2p_{1/2}$ (796.8 eV) (Shi et al. 2020), respectively. In addition, there are also two satellite peaks at 786.6 and 802.5 eV (identified as "Sat."), which have been proved to be the characteristic feature of high-spin divalent cobalt ions (Xu et al. 2015; Wang et al. 2020). Two peaks at 458.3 and 464.0 eV are correspond to Ti $2p_{3/2}$ and Ti $2p_{1/2}$ (Wang et al. 2013) in Fig. 2b. Meanwhile, the high-resolution spectrum displays the binding energy at 529.8 eV is fitted into O 1s (Fig. 2c). The EDS analysis of the LCT composite nanofibers in TEM mode is shown in Fig. 2d, which not only confirms the existence of Co, Ti, and O elements but also demonstrates the mass fraction and atomic fraction of the three elements in the attached table of the drawing. The atomic ratio of the elements Co:Ti:O is equal to 9.57:25.71:64.71. The Li element generally has no peak in EDS and other impurity elements like Cu and C are derived from the carbon film and copper mesh under TEM mode.

According to the XRD patterns of LCT composite nanofibers from Fig. 3a, several obvious diffraction peaks at 23.9°, 32.8°, 35.3°, 40.5°, 49.0°, 53.5°, 69.9°, and 63.5° correspond to the (012), (104), (110), (113), (024), (116), (214), and (300) lattice planes of $CoTiO_3$ in JCPDS card no. 15-0866, respectively. The diffraction peaks at 14.9°, 18.3°, 23.7°, 26.0°, 30.1°, 35.5°,

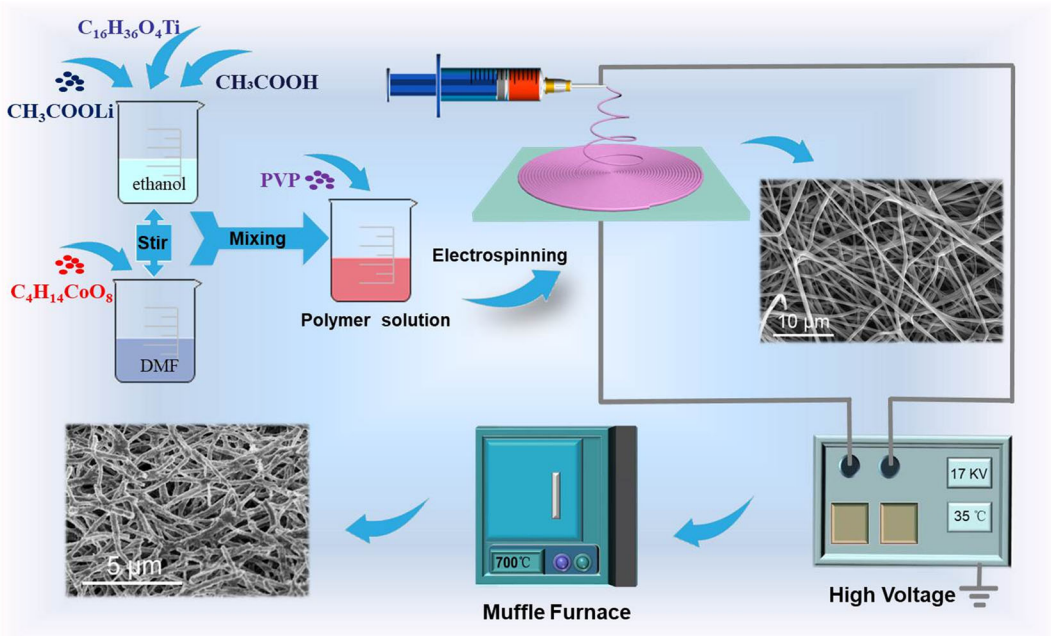

Fig. 1 Schematic illustration of the preparation processes of the materials

43.2°, 57.1°, and 62.7° can be assigned to the (110), (111), (210), (211), (220), (311), (400), (511), and (440) of $Li_2CoTi_3O_8$ (JCPDS card no. 49-0449), severally. And other diffraction peaks appearing at 27.4°, 36.1°, 41.2°, and 54.3° can be indexed to the (110), (101), (111), and (211) reflections of TiO_2 (JCPDS no. 21-1276), respectively. For $Li_2CoTi_3O_8$ nanofibers, all the diffraction peaks can be indexed to the $Li_2CoTi_3O_8$ phase (JCPDS no. 49-0449) (Fig. 3b).

The TG curves of LCT composite nanofibers are depicted in Fig. 3c, in which four weight losses are able to be found during heating from 25 to 720 °C. The 22% of weight loss is related to the evaporation of absorbed water when the temperature rises to 100 °C. The second weight loss (38%) is accompanied by an exothermic peak near 305 °C in the DTA curve between 180 and 310 °C because of the decomposition of lithium acetate, cobalt acetate and tetrabutyl titanate. The weight loss of 10% in the range of 310~370 °C can be ascribed to the decomposition of inorganic salt with an exothermic weak peak that appears near 360 °C in the DTA curve. The weight has lost 17% in the temperature range of 370 ~ 440 °C, mainly caused by the thermal decomposition of the PVP. Upon further heating from 440 to 720 °C, there is no obvious weight loss indicating that the decomposition reaction is completed with the total weight loss of 83%. The TG profiles of $Li_2CoTi_3O_8$ nanofibers are similar to LCT composite nanofibers (Fig. 3d), in which the weight loss of 20% in the range from 25 to 100 °C is related to the evaporation of absorbed water from the precursor fibers. The second weight loss (28%) between 180 and 305 °C is accompanied by an exothermic peak near 280 °C in the DTA curve because of the decomposition of lithium acetate, cobalt acetate, and tetrabutyl titanate. The third weight loss (18%) in the TG curve (305~370 °C) corresponds to the decomposition of inorganic salt appearing an exothermic weak peak near 314 °C in the DTA curve. The 17% of the last weight loss in the temperature changing from 370 to 410 °C suggests the thermal decomposition of the PVP. And then, no obvious weight loss from 410 to 720 °C shows the decomposition reaction is completed.

The morphology of LCT composite nanofibers is inspected by SEM (Fig. 4a, b), and the result shows that the LCT composite nanofibers have a uniform linear structure with the diameter of 150~200 nm after annealing. Transmission electron microscopy (TEM) is further implemented to verify the morphology and microstructure of the LCT composite fibers in Fig. 4c. Figure 4 d–f show that the crystallization interplanar spacings are closely related to the face (012) of $CoTiO_3$, the face (111) of $Li_2CoTi_3O_8$, and the face (111) of TiO_2, respectively. As demonstrated in Fig. 4g, the distinct

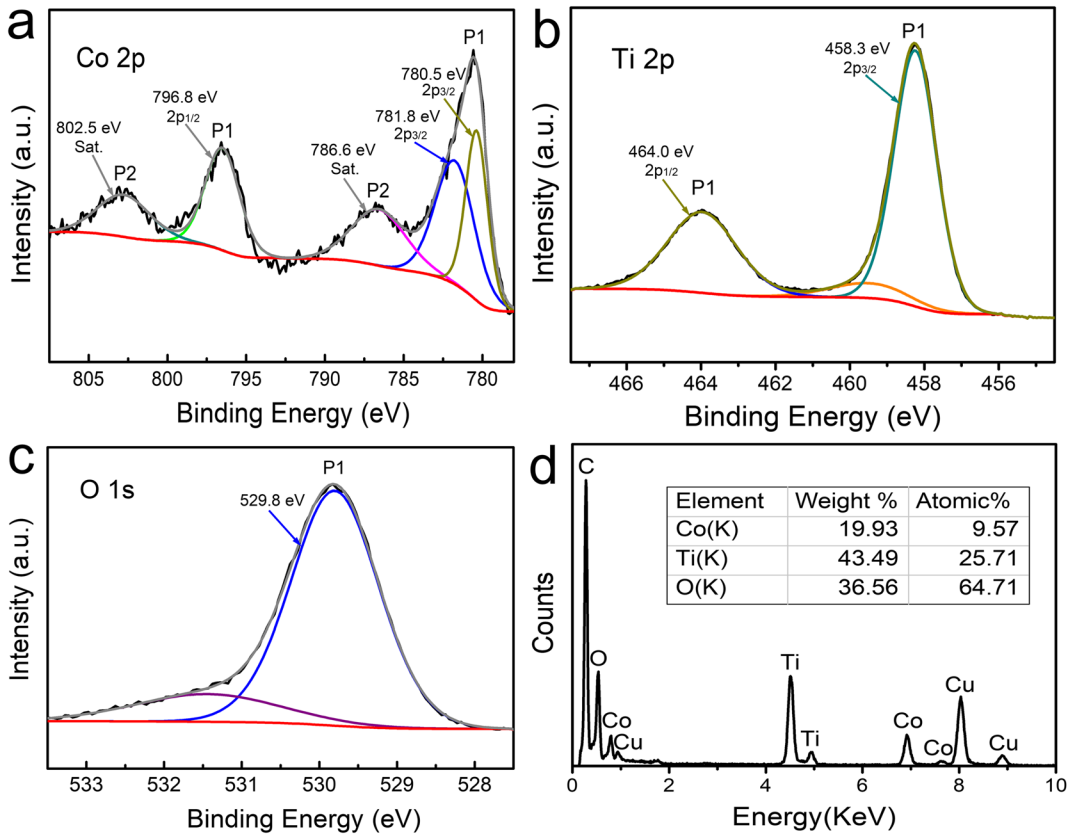

Fig. 2 High-resolution XPS spectra of **a** Co2p, **b** Ti2p, and **c** O1s for the LCT composite nanofibers. **d** EDS spectra

crystallization lattices indicate the $CoTiO_3$ materials have well crystallization with the neighboring plane spacing of 0.3705 nm, which can be assigned to the spacing plane d_{012} of the $CoTiO_3$ phase (JCPDS card no. 15-0866). Figure 4h displays that the prepared materials hold well crystallization with neighboring interplanar spacing of 0.4843 nm, which is assigned to the d_{111} spacing plane of the $LiCoTi_3O_8$ phase (JCPDS card no. 49-0449). The TiO_2 materials perfectly crystallize with plane spacing of 0.2175 nm in Fig. 4i attributed to the d_{111} plane of the TiO_2 phase (JCPDS card no. 21-1276). The above analysis results manifest that the composite nanofibers are a kind of complicated compound involving of $CoTiO_3$, $Li_2CoTi_3O_8$ and TiO_2. The elemental mapping analyses of composite nanofibers are illustrated in Fig. 4j–m, which reveal that the elements of Co, Ti, and O are distributed homogeneously in the whole nanofibers.

The electrochemical cycling performances of $Li_2CoTi_3O_8{\cdot}CoTiO_3{\cdot}TiO_2$ (LCT) composite nanofibers are described in Fig. 5a, in which the materials exhibit the first discharge capacity of 351.41 mAh g^{-1} at the current density of 100 mA g^{-1}. After 120 cycles of charge and discharge, the reversible lithium storage capacity of the LCT composite nanofibers has decreased to 201.68 mAh g^{-1}. The coulombic efficiency is close to 100% during the first 120 cycles of charge and discharge. As a comparison, the initial capacity of $Li_2CoTi_3O_8$ nanofibers achieves 408.88 mAh g^{-1} at the current density of 100 mA g^{-1}, while its reversible lithium storage capacity rapidly decreases to 90.23 mAh g^{-1} after 100 cycles (Fig. S2a). It clearly indicates that the LCT composite nanofibers hold higher reversible lithium storage capacity than the $Li_2CoTi_3O_8$ nanofibers. Therefore, it demonstrates that the unique composite structure is significant to enhance the rate capability of the materials.

As shown in Fig. 5b, cyclic voltammetry (CV) tests are carried out to evaluate the electrochemical activity of the LCT composite nanofibers. The interactions between with Li^+, $Li_2CoTi_3O_8$, $CoTiO_3$, and TiO_2 could be depicted by the following reactions (Wang et al. 2012; Jeong et al. 2014; Liu et al. 2017):

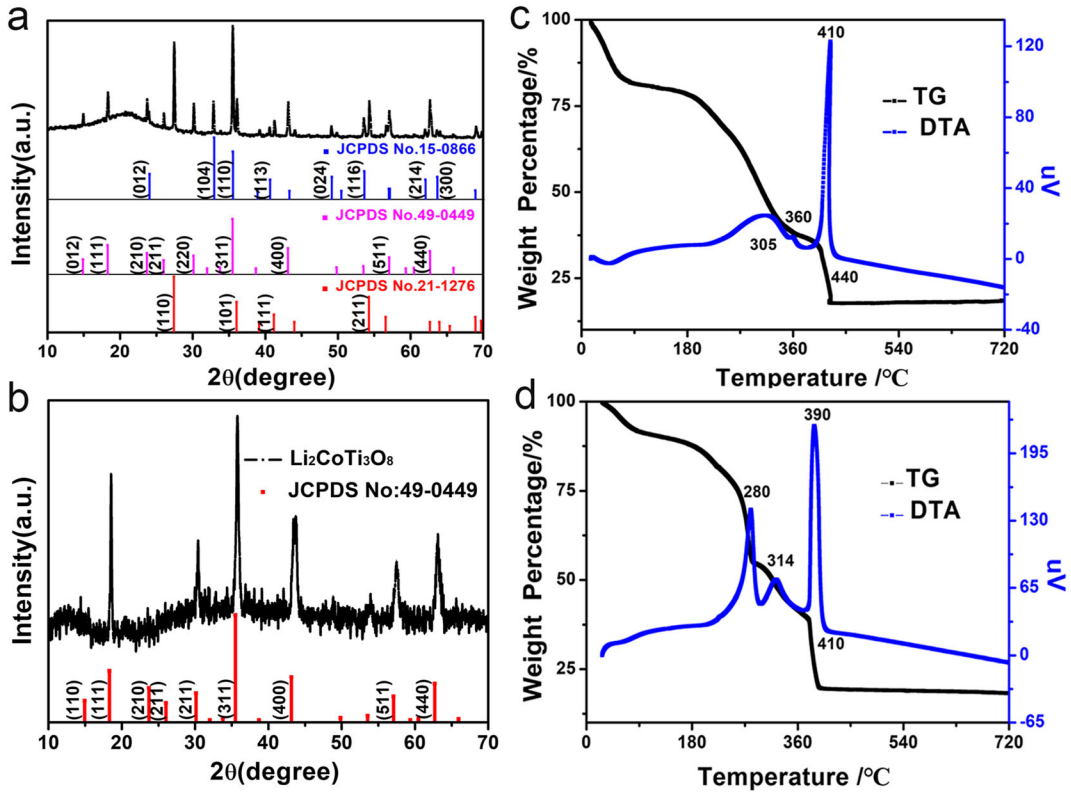

Fig. 3 XRD patterns of LCT composite nanofibers (**a**) and $Li_2CoTi_3O_8$ nanofibers (**b**). **c** TG-DTA curves of LCT composite nanofibers and **d** $Li_2CoTi_3O_8$ nanofibers

$$[LiCo_{0.9}]^{tet}[(LiCo_{0.1})Ti_3]^{oct}O_8 + 3e^- + 3Li^+ \leftrightarrow [Li_4]^{oct}[Co_{0.9}]^{tet}[(LiCo_{0.1})Ti_3]^{oct}O_8 \quad (1)$$

$$TiO_2 + xLi^+ + xe^- \leftrightarrow Li_xTiO_2\ (0 \le x \le 1) \quad (2)$$

$$CoTiO_3 + xLi^+ + xe^- \leftrightarrow Co + Li_xTiO_2 + Li_2O \quad (3)$$

During the first three cycles, the oxidation peak at 1.76 V indicates the process of LIBs' delithiation and two obvious reduction peaks at approximately 0.18 V and 0.17 V correspond to the lithium-ion intercalation process. For $Li_2CoTi_3O_8$ nanofibers, the oxidation peaks at 1.75 V and 0.16 V and reduction peak at about 0.3 V are shown in Fig. S3b.

It can be seen from Fig. 5c that the LCT composite nanofibers display the representative voltage profiles of charge/discharge curves at the current density of 100 mA g^{-1} with the potentials ranging from 0.0 to 3.0 V. The LCT composite nanofibers deliver an initial discharge capacity of 351.41 mAh g^{-1} and an initial charge capacity of 201.68 mAh g^{-1}, exhibiting superior electrochemical performances than other $Li_2CoTi_3O_8$-based composite materials (Table S1). After the first cycle, the irreversible capacity loss of 149.73 mAh g^{-1} mainly originates from the formation of the solid electrolyte interphase (SEI) film (Huff et al. 2016). At the same circumstances, the charge/discharge voltage profiles of $Li_2CoTi_3O_8$ nanofibers perform the initial discharge capacity of 408.88 mAh g^{-1} and initial charge capacity of 181.64 mAh g^{-1} with the irreversible capacity loss of 227.24 mAh g^{-1} (Fig. S3a).

Figure 5d shows the rate performances of the LCT composite nanofibers at different current densities from 100 to 800 mA g^{-1}. The initial reversible capacity of the composite nanofibers is 196.45 mAh g^{-1} at the current density of 100 mA g^{-1}. Subsequently, the charge capacities reduce slowly to 171.36, 148.35, 134.14, 121.67, 110.63, 101.57, and 97.14 mAh g^{-1} when the current densities gradually increase to 200, 300, 400, 500, 600, 700, and 800 mA g^{-1}, respectively. Upon the current

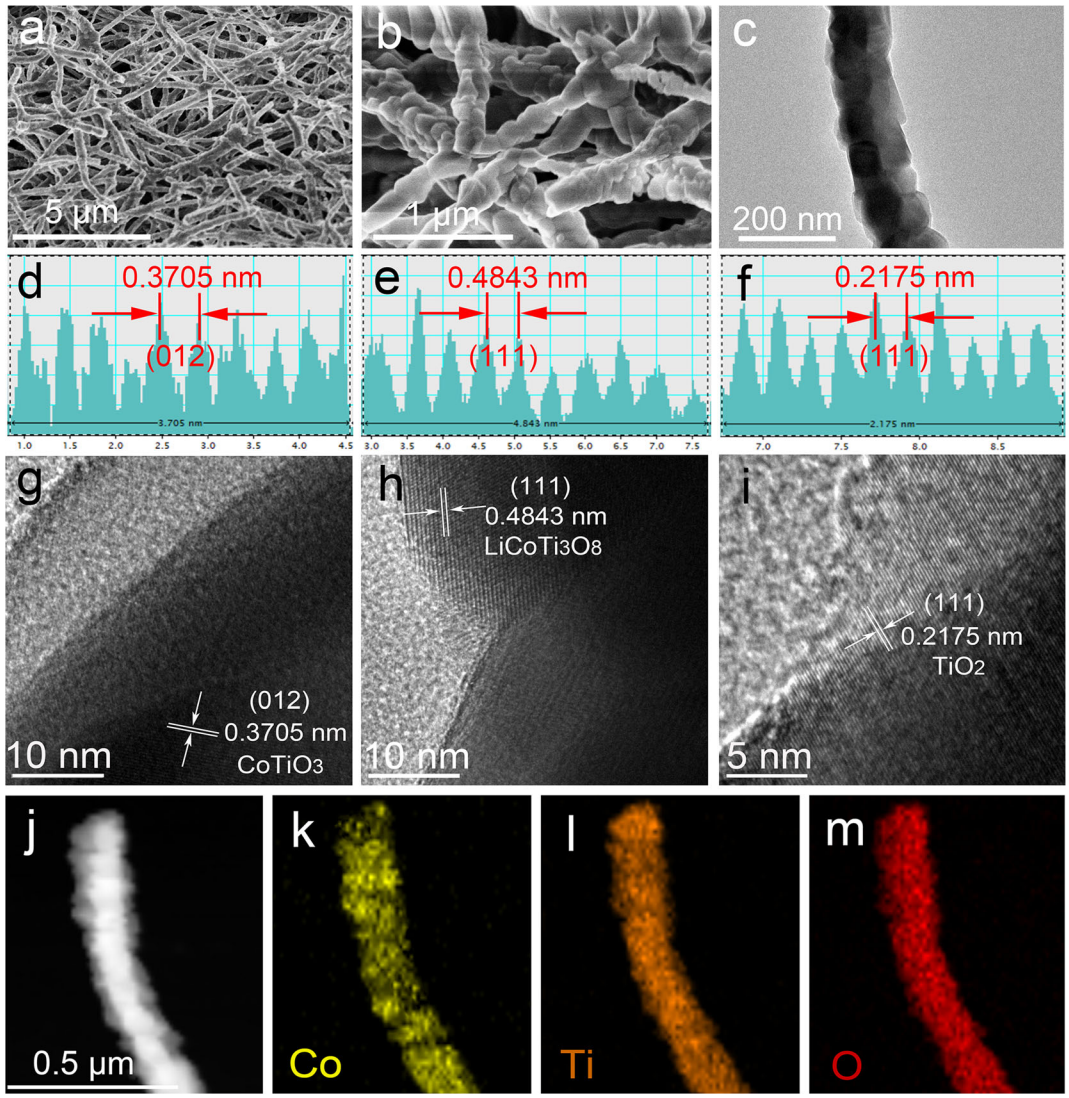

Fig. 4 **a**, **b** SEM images of the LCT composite nanofibers. **c** HRTEM image of composite nanofibers. **d**–**f** Interplanar crystallized spacing statistical tables. **g**–**i** HRTEM images. **j**–**m** Elemental mapping images of Co, Ti, and O

density turns back to 100 mA g^{-1}, the charge capacity of the composite nanofibers can still recover to 185.59 mAh g^{-1}. By contrast, the rate performances of $Li_2CoTi_3O_8$ nanofibers are revealed in Fig. S2b, where $Li_2CoTi_3O_8$ nanofibers present low charge capacities of 130.15, 120.27, 111.35, 102.34, 97.83, 95.10, 90.12, 85.38, 80.16, and 141.13 mAh g^{-1} at the current densities of 50, 100, 200, 300, 400, 500, 600, 700, 800, and 50 mA g^{-1}, respectively. As shown in Fig. 5e, when the high current density of 1000 mA g^{-1} is exerted, the capacity of the composites gradually increases from 61.72 to 110.35 mAh g^{-1} before 300 cycles, and then decreases to 62.39 mAh g^{-1} in the next 500 cycles, which can be regarded as the reason of the activation process of the materials. All the above special rate performances may result from the following aspects: (i) the one-dimensional (1D) nanostructures provide sufficiently large interface areas between electrodes and electrolyte for the Li^+ rapid transfer during lithiation/delithiation; (ii) the advantageous structures of nanocomposites relieve volume changes and pulverization of the materials during cycling; (iii) the ternary

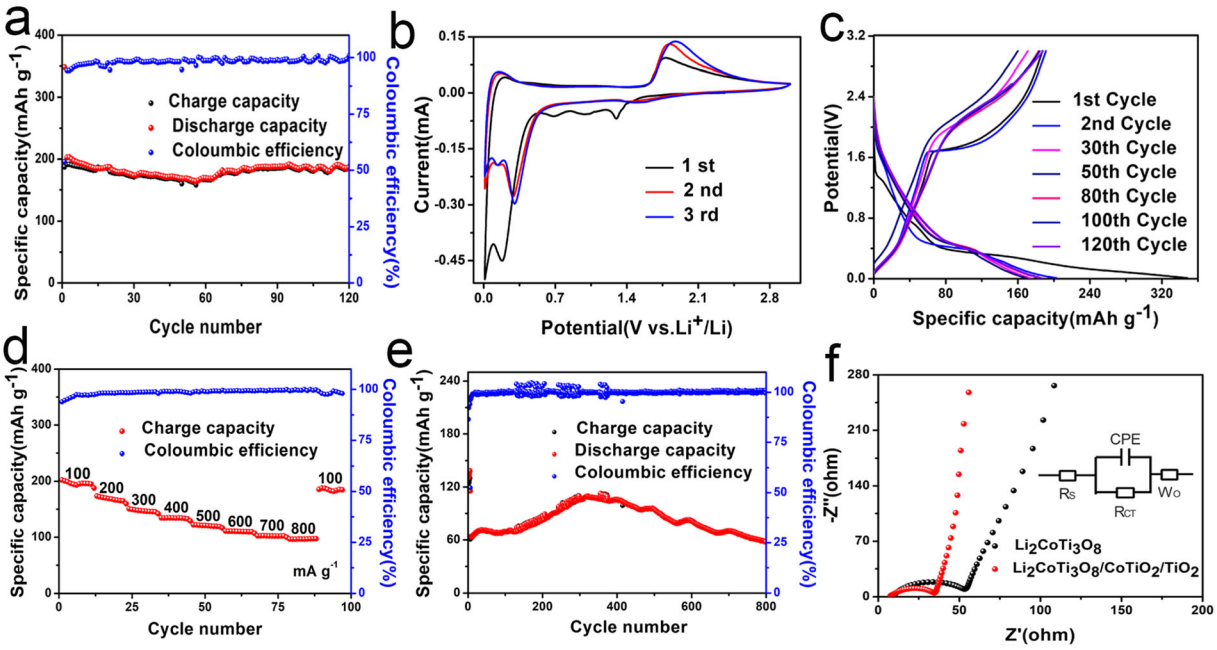

Fig. 5 **a** The cycling properties of LCT composite nanofibers at current densities of 100 mA g^{-1}. **b** Cyclic voltammograms curves at a scan rate of 0.1 mV s^{-1} from 0.01 to 3.00 V. **c** Charge/discharge curves of at current densities of 100 mA g^{-1}. **d** Rate capabilities of. LCT composite nanofibers. **e** Charge/discharge curves at current densities of 1000 mA g^{-1}. **f** EIS patterns for the LCT composite nanofibers and $Li_2CoTi_3O_8$ nanofibers

composite materials $Li_2CoTi_3O_8{\cdot}CoTiO_3{\cdot}TiO_2$ can play a synergistic role in improving electrochemical properties effectively.

To further improve electrochemical performances, electrochemical impedance spectroscopy (EIS) analyses of the nanofibers are performed at room temperature, of which the EIS curves are shown in Fig. 5f. The intercepts of the Nyquist plots at the high-frequency regions can be attributed to the bulk resistance of the liquid electrolyte (Re), whereas the semicircle in the medium frequency regions is the charge-transfer resistance (Rct) of the electrode/electrolyte interfaces. Meanwhile, the line in the low-frequency region corresponds to the diffusion limitation within the electrodes. CPE is defined as a constant phase element, and W_0 represents Warburg impedance. The equivalent circuit diagram can perfectly match the EIS test results (Fig. 5f). The fitting results are shown in Table 1, where it has been observed that the Rct of LCT composite nanofibers (26.91 Ω) is much smaller than that of Li_2CoTi_3O nanofibers (41.35 Ω). Moreover, the Rs of LCT composite nanofibers (7.95 Ω) is also lower than that of Li_2CoTi_3O nanofibers (9.18 Ω), indicating that the electrical conductivities of LCT composite nanofibers are superior to that of Li_2CoTi_3O nanofibers.

Conclusions

In summary, LCT composite nanofibers were synthesized feasibly by the electrospinning method and characterized by XRD, TG-DTA, SEM, TEM, XPS, EDS, CV, and so on. After 120 cycles, the tests show that LCT composite nanofibers as LIBs anode materials can retain a reversible capacity of 201.68 mAh g^{-1} at the current density of 100 mA g^{-1}. The electrochemical performances exhibit large cycle capacity and high rate capability, in which the combined composite materials can achieve superior performances. This work provides splendid ideas for the fabrication of different composite materials, and the synthesized LCT composite nanofibers can be considered as promising candidates for optimal anode materials for LIBs.

Table 1 The fitting results of LCT composite nanofibers and $Li_2CoTi_3O_8$ nanofibers

Fitting results of EIS		
Sample	Rs (Ω)	Rct (Ω)
LCT composite nanofibers	7.95	26.91
$Li_2CoTi_3O_8$ nanofibers	9.18	41.35

Funding information The work was supported by the National Natural Science Foundation of China (21571110), the NSF of Zhejiang province (LY18B010003), the NSF of Ningbo (2019A610002), the Foundation of State Key Laboratory of Structural Chemistry (FJIRSM, CAS, 20190028), and the K. C. Wong Magna Fund in Ningbo University.

Compliance with ethical standards

Conflict of interest The authors declare that they have no conflict of interest.

References

Ahn D, Xiao XC (2011) Extended lithium titanate cycling potential window with near zero capacity loss. Electrochem Commun 13:796–799

Bhardwaj N, Kundu SC (2010) Electrospinning: a fascinating fiber fabrication technique. Biotechnol Adv 28:325–347

Cheng Z, Hu Y, Wu K, Xing Y, Pan P, Jiang L, Mao J, Ni C, Wang Z, Zhang M, Zhang Y, Gu X, Zhang X (2020) Si/TiO_2/Ti_2O_3 composite carbon nanofiber by one-step heat treatment with highly enhanced ion/electron diffusion rates for next-generation lithium-ion batteries. Electrochim Acta 337: 135789

Cusenza M, Bobba S, Ardente F, Cellura M, Persio F (2019) Energy and environmental assessment of a traction lithium-ion battery pack for plug-in hybrid electric vehicles. J Clean Prod 215:634–649

Goriparti S, Miele E, Angelis F, Fabrizio E, Zaccaria P, Capigliaa C (2014) Review on recent progress of nanostructured anode materials for Li-ion batteries. J Power Sources 257:421–443

Han Y, Huang GY, Xu SM (2019) Structural reorganization-based nanomaterials as anodes for lithium-ion batteries: design, preparation, and performance. Small 16:1902841

He ZX, Jiang YQ, Zhu J, Li YH, Jiang Z, Zhou HZ, Meng W, Wang L, Dai L (2017) Boosting the performance of $LiTi_2(PO_4)_3$/C anode for aqueous lithium ion battery by Sn doping on Ti sites. J Alloys Compd 731:32–38

Hou L, Qin X, Gao XJ, Guo T, Li X, Li J (2018) Zr^{-}doped $Li_4Ti_5O_{12}$ anode materials with high specific capacity for lithium-ion batteries. J Alloys Compd 774:38–45

Huang B, Pan Z, Su X, An L (2018) Recycling of lithium-ion batteries: recent advances and perspectives. J Power Sources 399:274–286

Huff L, Tavassol H, Esbenshade J, Xing WT, Chiang YM, Gewirth A (2016) Identification of Li-ion battery SEI compounds through ^{7}Li and ^{13}C solid-state MAS NMR spectroscopy and MALDI-TOF mass spectrometry. ACS Appl Mater Interfaces 8:371–380

Jeong J, Junge D, Shin E, Oh E (2014) Boron-doped TiO_2 anode materials for high-rate lithium ion batteries. J Alloys Compd 604:226–232

Jung JW, Lee C, Yu S, Kim I (2015) Electrospun nanofibers as a platform for advanced secondary batteries: a comprehensive review. J Mater Chem A 10:703–750

Kamali A, Fray D (2015) Electrochemical interaction between graphite and molten salts to produce nanotubes, nanoparticles, graphene and nanodiamonds. J Mater Sci 51:569–576

Lao MM, Qian SS, Yu HX, Yan L, Li P, Lin XT, Long NB, Shui M, Shu J (2016) Enhanced electrochemical properties of Mg^{2+} doped $Li_2Na_2Ti_6O_{14}$ anode material for lithium-ion batteries. Electrochim Acta 2016(196):642–652

Leng MZ, Bi JQ, Wang WL, Liu R, Xia C (2019) Synthesis and characterization of Ru doped $NaNi_{0.5}Mn_{0.3}Ti_{0.2}O_2$ cathode material with improved electrochemical performance for sodium-ion batteries. Ionics 25:1105–1115

Liu SY, Fan CY, Wang HC, Zhang JP, Wu XL (2017) Electrochemical in situ formation of a stable Ti-based skeleton for improved Li-storage properties: a case study of porous $CoTiO_3$ nanofibers. Chem Eur J 23:8712–8718

Liu H, Wu XN, Guo EY, Lu QF (2019a) Tailored synthesis of coral-like $CoTiO_3$/Co_3O_4/TiO_2 nanobelts with superior Lithium storage capability. Energy Technol 8:1900774

Liu HD, Zhu ZY, Huang J, He X, Chen Y, Zhang R, Lin RQ, Li YJ, Yu S, Xing X, Yan QZ, Li XG, Frost M, An K, Feng J, Kostecki R, Xin HL, Ong S, Liu P (2019b) Elucidating the limit of Li insertion into the spinel $Li_4Ti_5O_{12}$. ACS Mater Lett 1:96–102

Ouyang CY, Zhong ZY, Lei MS (2007) Ab initio studies of structural and electronic properties of $Li_4Ti_5O_{12}$ spinel. Electrochem Commun 9:1107–1112

Railey P, Song Y, Liu TY (2017) Metal organic frameworks with immobilized nanoparticles: synthesis and applications in photocatalytic hydrogen generation and energy storage. Mater Res Bull 96:385–394

Sandhya C, John P, Gouri C (2014) Lithium titanate as anode material for lithium-ion cells: a review. Ionics 20:601–620

Serife E, Stojanovska E, Simon B, Kilic A (2015) A review of nanofibrous structures in lithium ion batteries. J Power Sources 300:199–215

Shi JM, Liu GZ, Weng W, Cai LT, Zhang Q, Wu JH, Xu XX, Yao XY (2020) Co_3S_4@$Li_7P_3S_{11}$ hexagonal platelets as cathodes with superior interfacial contact for all-solid-state lithium batteries. ACS Appl Mater Interfaces 12:14079–14086

Simon G, Goswami T (2011) Improving anodes for lithium ion batteries. Metall Mater Trans A 42:231–238

Tian BB, Xiang HF, Zhang L, Wang HH (2012) Effect of Nb-doping on electrochemical stability of $Li_4Ti_5O_{12}$ discharged to 0 V. J Solid State Electrochem 16:205–211

Tojo T, Kawashiri S, Tsuda T, Kadowaki M, Inada R, Sakuraib Y (2019) Electrochemical performance of single $Li_4Ti_5O_{12}$ particle for lithium ion battery anode. J Electroanal Chem 836: 24–29

Trong L, Thao T, Dinh N (2015) Characterization of the Li-ionic conductivity of $La_{(2/3-x)}Li_{3x}TiO_3$ ceramics used for all-solid-state batteries. Solid State Ionics 278:228–232

Wang L, Xiao QZ, Li ZH, Lei GT, Wu LJ, Zhang P, Mao J (2012) Synthesis of $Li_2CoTi_3O_8$ fibers and their application to lithium-ion batteries. Electrochim Acta 77:77–82

Wang J, Zhao HL, Shen YN, Du ZH, Chen XM, Xia Q (2013) Structure, stoichiometry, and electrochemical performance of $Li_2CoTi_3O_8$ as an anode material for lithium-ion batteries. Chempluschem 78:1530–1535

Wang J, Shen LF, Li HS, Ding B, Nie P, Dou H, Zhang XG (2014) Mesoporous $Li_4Ti_5O_{12}$/carbon nanofibers for high-rate lithium-ion batteries. J Alloys Compd 587:171–176

Wang ZY, Xiong FY, Tao HZ, Yue YZ (2020) Revealing the role of the amorphous phase in $Na_{0.74}CoO_2$/C/N composite cathode. J Alloys Compd 815:152616

Xu JQ, Thomas H, Francis R, Lum K, Wang JW, Liang B (2007) A review of processes and technologies for the recycling of lithium-ion secondary batteries. J Power Sources 177:512–527

Xu HH, Sun YM, Luo W, Chen CJ, Liu Y, Huang YH (2014) Highly porous $Li_4Ti_5O_{12}$/C nanofibers for ultrafast electrochemical energy storage. Nano Energy 10:163–171

Xu M, Han L, Han YJ, Yu Y, Zhai JF, Dong SJ (2015) Porous CoP concave polyhedron electrocatalysts synthesized from metal-organic frameworks with enhanced electrochemical properties for hydrogen evolution. J Mater Chem A 3: 21471–21477

Yi TF, Yang SY, Li XY, Yao JH, Zhu YR, Zhu RS (2014a) Submicrometric $Li_{4-x}Na_xTi_5O_{12}$ ($0 \le x \le 0.2$) spinel as anode material exhibiting high rate capability. J Power Sources 246: 505–511

Yi TF, Yang SY, Zhu YR, Ye M, Xie Y, Zhu RS (2014b) Enhanced rate performance of $Li_4Ti_5O_{12}$ anode material by ethanol-assisted hydrothermal synthesis for lithium-ion battery. Ceram Int 40:9853–9858

Yuan T, Yu X, Cai R, Zhou YK, Shao ZP (2010) Synthesis of pristine and carbon-coated $Li_4Ti_5O_{12}$ and their low-temperature electrochemical performance. J Power Sources 195:4997–5004

Zeng LC, Qiu L, Cheng HM (2019) Towards the practical use of flexible lithium ion batteries. Energy Storage Mater 23:434–438

Zhang QY, Lu HS, Zhong HX, Yan XD, Ouyang CY, Zhang LZ (2015) W^{6+} & Br^- codoped $Li_4Ti_5O_{12}$ anode with super rate performances for Li-ion batteries. J Mater Chem A 3:13706–13716

Zhang PC, Yuan T, Pang YP, Peng CX, Yang JH, Ma ZF, Zheng SY (2019) Influence of current density on graphite anode failure in lithium-ion batteries. J Electrochem Soc 166: A5489–A5495

Zhao Z, Xu YL, Ji MD, Zhang H (2013) Synthesis and electrochemical performance of F^- doped $Li_4Ti_5O_{12}$ for lithium-ion batteries. Electrochim Acta 109:645–650